Estratto da:

Annali di Chimica, 1997
Società Chimica Italiana,
Viale Liegi 48 - Roma

ADVANCES IN SCANNING ELECTROCHEMICAL MICROSCOPY

Allen J. BARD (°), David E. CLIFFEL, Christophe DEMAILLE,
Fu-Ren F. FAN, and Michael TSIONSKY

Department of Chemistry and Biochemistry, University of Texas at Austin,
Austin, Texas 78712

Summary -The principles of scanning electrochemical microscopy (SECM) will be briefly introduced, and recent advances using this technique will be discussed. Recent studies from our group using SECM include the characterization of thin films, using the SECM in combination with a quartz-crystal microbalance; the detection of single molecules; the determination of electron-transfer rates the interface between two immiscible electrolyte solutions; and the measurement of the kinetics of ECE and DISP1 reactions.

Riassunto - I principi della microscopia elettrochimica a scansione (SECM) viene introdotta in sommario, e vengono discussi gli sviluppi più recenti di questa tecnica. Studi recenti di applicazioni della SECM hanno riguardato la caratterizzazione di film sottili, con l'uso combinato di una microbilancia a cristallo di quarzo ; il rilevamento di singole molecole ; la determinazione di velocità di trasferimento elettronico all'interfaccia tra due soluzioni immiscibili di elettroliti ; e la misura della cinetica delle reazioni ECE e DISP1.

(°), Author to whom correspondence should be directed.

INTRODUCTION

Scanning electrochemical microscopy (SECM) was developed in our laboratory beginning in 1989[1] as a technique which combines the electrochemical properties and advantages of an ultramicroelectrode[2] with the high resolution scanning ability and positioning capabilities of the scanning tunneling microscope (STM). There have been a number of reviews covering the principles and applications of SECM,[3-7] so we will only briefly review the basics and apparatus. This paper focuses on recent experiments being carried out in our laboratory using this technique.

SECM principles

The SECM is based on the changes in the faradaic current that flows during a redox process at a tip as it moves above a substrate that is immersed in a solution containing an appropriate species in the oxidized (Ox) or reduced (Red) state. The potential of the tip is controlled by a potentiostat and the solution is held in an electrochemical cell containing the tip, auxiliary and reference electrodes. If the solution contains the species Ox and the tip potential is adjusted with respect to the reference electrode to reduce Ox at a mass-transfer-controlled rate, the reaction Ox + $ne \rightarrow$ Red occurs. If the ultramicroelectrode tip is far from any substrate, the steady-state current that flows, $i_{T,\infty}$, is given by equation 1:[2]

$$i_{T,\infty} = 4nFDca \qquad (1)$$

where F is the Faraday, c is the concentration of Ox, D is its diffusion coefficient, and a is the radius of the tip. This current represents the flux of Ox to the electrode through the essentially hemispherical diffusion layer around the tip. However, when the tip is close to the substrate, i.e., within a few tip radii, the current is perturbed by the presence of the substrate. If the reverse reaction Red $\rightarrow$ Ox + ne cannot occur on the substrate, e.g., if the substrate is an electrical insulator that does not react with Red, the current will be smaller than $i_{T,\infty}$, because the substrate blocks the diffusion of Ox to the tip; this effect is termed negative feedback. For a conductive substrate, the oxidation of Red to Ox can occur. This provides an additional source of Ox for the tip, and the current observed is greater than $i_{T,\infty}$; i.e., positive feedback is observed. These principles are illustrated in Figure 1.

In general, in SECM the relative magnitude of the current (i_T) compared to $i_{T,\infty}$ is a measure of the distance between the tip and substrate, d, and depends upon the nature of the substrate. The theoretical behavior of SECM is readily accessible through typical electrochemical diffusion-kinetic treatments.[3, 8-13] Dimensionless curves of $i_T/i_{T,\infty}$ versus d/a, which are independent of solution concentration and diffusion coefficient, can be plotted. Figure 2 shows the predicted behavior for an unreactive insulator (i.e., a material where the rate constant, k_f, of the Red $\rightarrow$ Ox reaction is 0) and for a conductive substrate (where $k_f \rightarrow \infty$). Thus by measuring the $i_T/i_{T,\infty}$ ratio, one can immediately estimate the tip-substrate distance d, if the tip radius a is known. When the rate constant of the Red $\rightarrow$ Ox reaction is of an intermediate value, i.e., $0 < k_f < \infty$, a family of curves[11,14] is obtained which spans the behavior between the two limits illustrated in Figure 2.

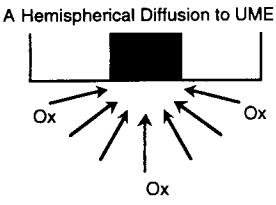

FIG. 1 - Basic principles of SECM substrate, diffusion leads t substrate. Hindered diffus Positive feedback leads to

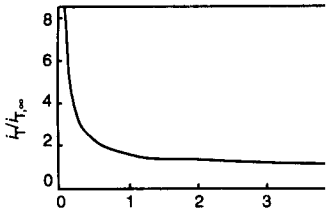

FIG. 2 - Normalized tip current as a conductive substrate and

The basic apparatus used for SECM Thus a potentiostat (or a bipotentiostat, i tip potential with respect to the reference substrate (the z direction) and across the scanners. Tip potential and position are D/A cards. This arrangement allows one scans showing i_T at a given d as a functio and constant current operation are also p

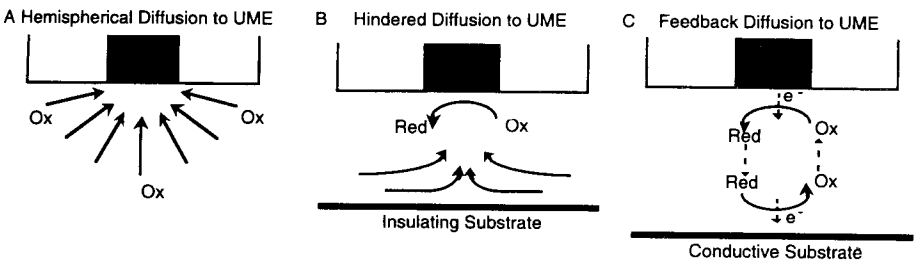

FIG. 1 - Basic principles of SECM. (A) With the ultramicroelectrode (UME) tip far from substrate, diffusion leads to a steady-state current $i_{T,\infty}$. (B) UME near an insulating substrate. Hindered diffusion leads to $i_T < i_{T,\infty}$. (C) UME near a conductive substrate. Positive feedback leads to $i_T > i_{T,\infty}$.

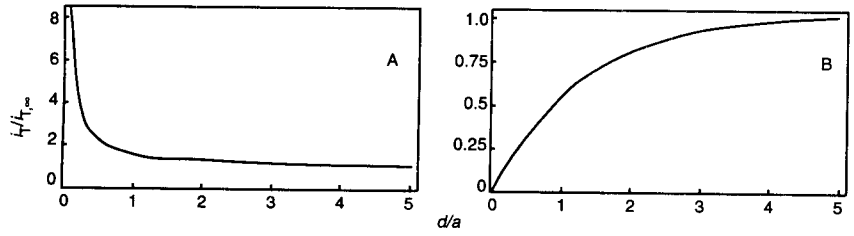

FIG. 2 - Normalized tip current as a function of dimensionless tip-substrate separation for (A) a conductive substrate and (B) an unreactive insulating substrate.

The basic apparatus used for SECM[1,6] combines electrochemical and STM instrumentation. Thus a potentiostat (or a bipotentiostat, if the substrate potential is controlled) is used to adjust the tip potential with respect to the reference electrode. The tip is moved toward and away from the substrate (the *z* direction) and across the surface (*x* and *y* directions) by means of piezoelectric scanners. Tip potential and position are adjusted via a digital computer and the associated A/D and D/A cards. This arrangement allows one to obtain approach curves of $i_T/i_{T,\infty}$ versus d/a, and surface scans showing i_T at a given d as a function of x,y position. SECM scans with tip position modulation and constant current operation are also possible.[15,16]

DISCUSSION

SECM coupled with a quartz crystal microbalance (SECM-QCM)

The use of SECM for characterizing thin films has been described,[5] but these studies often involve several complex processes and additional information on the nature of the thin films is required. The quartz crystal microbalance is capable of monitoring the mass and viscoelasticity of a thin film. In electrochemical QCM, a piezoelectric quartz crystal with gold or platinum electrodes on each side is used as a substrate. Typically, the electrochemical current of the electrode is recorded as a function of time or potential, while the resonant high frequency (5 MHz) of the quartz is monitored by an oscillator circuit. The QCM resonant frequency is inversely related to the electrode mass, including any thin layers on top of the electrode. The previous combination of SECM-QCM used only a single potentiostat to control the tip-substrate potential in mapping the sensitivity of the QCM.[17] By adding a bipotentiostat to independently control the tip and substrate potentials, the combined technique offers a better way to study thin films than by either of the techniques alone. The use of SECM-QCM should be applicable to a number of electrochemical problems: the nature of corrosion processes (passivation layer growth or etching), ion and solvent transport between the thin film and electrolyte, and film dissolution.

The electrodeposition and etching of copper and silver deposited on the QCM substrate electrode was used to characterize the SECM-QCM instrumentation. The conditions were similar to previous SECM copper etching experiments where the etching was confirmed ex-situ by scanning electron microscopy.[18] The copper layer was electrochemically deposited from 5 mM copper sulfate in 0.2 M sulfuric acid onto a gold QCM substrate electrode by application of a potential step. The deposition solution was removed from the cell, the cell was rinsed with water, and then the etching solution of 1-2 mM $Fe(phen)_3^{2+}$ in 10 mM acetate buffer (pH 4.0) was added. The QCM clearly showed that this solution could slowly etch the copper layer itself, but the pH stability range of the copper layer around pH 5.0 is very narrow; so silver layers were used. A much greater stability was observed in the etching solution of 60 mM $Fe(bpy)_3SO_4$ in 0.2 M Na_2SO_4. With the high concentration of etchant, $Fe(bpy)_3^{3+}$, generated at a 0.1 mm Pt electrode, in-situ etching could be confirmed by observing the increase in QCM frequency while the substrate was at open circuit. A schematic of the etching process is shown in Figure 3.

As predicted by Hillier and Ward,[19] the sensitivity of the QCM response to metal etching depended on tip location. The relative QCM response was greatest when the tip was over the center of the deposited layer. The response also depended on the thickness of the silver layer; a thicker layer distorted the sensitivity by giving a higher center response and lower edge sensitivity. For many thin-film studies using SECM-QCM, the higher sensitivity in the center of the substrate layer could be used to obtain better signal-to-noise by positioning the SECM tip above the center of the QCM electrode. This method demonstrates a new operation mode of tip generation (monitoring current) and substrate collection (monitoring frequency). Unfortunately, relatively large tip electrodes and high concentrations are needed for the SECM tip to cause discernible changes in the QCM frequency.

Metal
Film

FIG. 3 - Schematic of the etchin
the SECM-QCM.

SECM-QCM can also be used to
film as the potential of the thin film o
frequency (Figure 4C) are recorded to
corresponding solution changes. As a
evaporated onto a QCM gold electrod
previously been studied using SECM[1

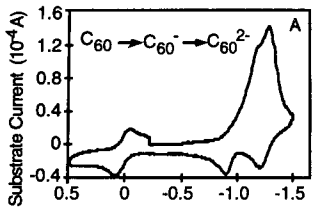

FIG. 4 - SECM-QCM results of
ferrocene as a potential
two C_{60} reduction wav
the tip held at -0.05 V;
ferrocene. (C) QCM s
monoanion and the dep

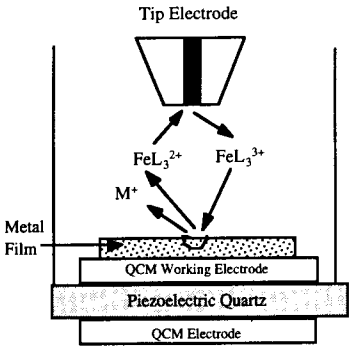

FIG. 3 - Schematic of the etching of a metal (copper or silver) layer by iron complexes using the SECM-QCM.

SECM-QCM can also be used to monitor changes in the solution adjacent to an electroactive film as the potential of the thin film on a substrate is changed. The substrate current (Figure 4A) and frequency (Figure 4C) are recorded to monitor film behavior while the tip current (Figure 4B) shows corresponding solution changes. As an example, fullerene (C_{60}) thin films of 3-5 μm particles were evaporated onto a QCM gold electrode for SECM-QCM experiments. C_{60} thin films have previously been studied using SECM[19] and QCM[20] separately and a general review is available.[21]

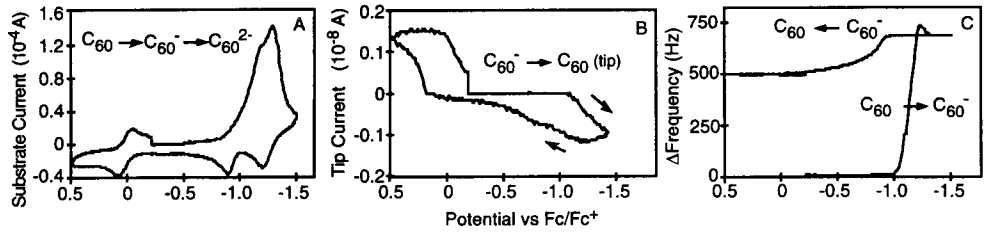

FIG. 4 - SECM-QCM results of a C_{60} thin film in 30 mM KCF_3SO_3/acetonitrile with ferrocene as a potential reference. (A) Substrate cyclic voltammetry at 50 mV/s; the two C_{60} reduction waves are not clearly separated. (B) Tip collection current with the tip held at -0.05 V; note the collection of ferrocenium when the substrate oxidizes ferrocene. (C) QCM substrate frequency change showing dissolution of the monoanion and the deposition of the film upon reversal.

Because the solubility of C_{60} anions is much greater with potassium cation than with tetra-alkylammonium cation electrolytes, potassium triflate in acetonitrile solution was used to study C_{60} films. Thus, reprecipitation of initially dissolved C_{60}^- species was minimized, leading to a clearer interpretation of the QCM substrate frequency (mass) and tip current results. SECM-QCM studies of the C_{60} film confirm the findings of the separate SECM and QCM studies; i.e., the reduction of a C_{60} film (Figure 4A) results in the nearly complete dissolution of C_{60}^-. This is shown by the re-oxidation current at the tip electrode (Figure 4B) and by the frequency increase (i.e., mass loss) of the QCM substrate (Figure 4C). The diffusional delay time for the anions to cross the tip-substrate gap is responsible for the delay in the tip current of Figure 4B. Because the second reduction, of C_{60}^- to C_{60}^{2-}, is completely a solution wave, there is no effect on QCM frequency (Figure 4C). Upon the reversal of the scan direction, the two solution oxidation waves are clearly distinct, with the second oxidation, from C_{60}^- to C_{60} film showing an increase in substrate mass (Figure 4C). Subsequent reduction of the film on the tip occurs at the same potential as on the substrate, indicating no change in composition.

Thin particle films of a *t*-butylcalix[8]arene-C_{60} complex were also studied using SECM-QCM. This complex is insoluble in all known solvents and is known to be a "ball in a basket" structure,[22] but little was known about the effect of complexation on the electrochemically active C_{60} within the film. The SECM-QCM experiment indicates that the reduction of the film results in the breaking apart of the complex; the insoluble calixarene remains on the substrate surface, and the soluble fullerene anions dissolve into the acetonitrile. The tip electrode detected a re-oxidation current when the calixarene-C_{60} film was reduced, and the QCM indicated a mass loss that coincided with the reduction. The magnitude of the frequency shift of the QCM and the subsequent potential scan of the film collected on the tip indicated that only the C_{60} had been lost from the film as a result of the reduction. An approach curve taken with the tip after the reduction of the calixarene-C_{60} film showed that the calixarene remained on the QCM substrate electrode. The tip current became smaller as the tip approached the calixarene-covered film, indicating a partially insulating film. Thus, in both cases, the reduction of these films results in the dissolution of C_{60} anions from the film.

The combination of QCM with SECM provides new information about the mass changes occurring in electrochemically active thin films and might yield information about viscoelasticity changes as well. This could be very important for polymer film studies where the movement of ions and solvent are part of the electrochemical process.

Single-molecule detection with the SECM

The use of small SECM tips of an appropriate geometry and the positive feedback mode have made possible the trapping and detection of single molecules.[23-25] The single-molecule trapping experiments require a tip with a diameter of the order of 10-20 nm and the particular geometry that results from the procedure used in tip preparation. The tip is made by electrochemical sharpening of a Pt-Ir (80%-20%) wire (0.250-mm diameter), which is completely insulated by passing it through molten Apiezon wax or polyethylene.[26] A hole is then produced at the very end by mounting the tip in the SECM apparatus and moving it toward the substrate until a current of the order of a few picoamperes flows. This produces a tip that shows an approach curve such as that shown in curve 3 of Figure 5A; this curve suggests a geometry very different than that of a disk electrode in a plane, which produces curves 1 and 2 in Figure 5 a tip that is slightly recessed within the ins schematically in Figure 5B.[24] The decreas Figure 5A is largely due to diffusion of re by a decrease in the area of the conductor

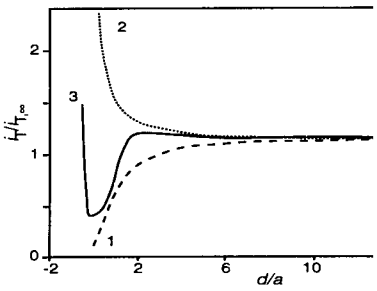

FIG. 5 - (A) SECM approach curve shaped tip, conductive sub Schematic of single-molecu between tip and substrate.

It is not currently possible to measur at an electrode. To detect a single molecul process. In the SECM experiment, illustra positive feedback process, i.e., the repeate substrate as the molecule, in the oxidized substrate. The transport between the two between tip and surface separated by a dis redox species). If d = 10 nm and $D = 10^{-5}$ per second. If each cycle results in the exc current of about 1.6 pA will flow. Thus pc that results in a readily measurable curren small pocket formed by the surrounding ir time to make the measurement, and this is

Figure 6A shows an experiment with oxidized at the tip to produce the ferrocen substrate.[23] In this experiment, the tip wi the tip current (see curve 3 of Figure 5A)

which produces curves 1 and 2 in Figure 5A. A reasonable fit to this curve is obtained by simulating a tip that is slightly recessed within the insulating film of wax to form a small pocket, as shown schematically in Figure 5B.[24] The decrease in the current at close approach as shown in curve 3 of Figure 5A is largely due to diffusion of redox species to the tip being hindered by the substrate and by a decrease in the area of the conductor as the wax is squeezed against the substrate.

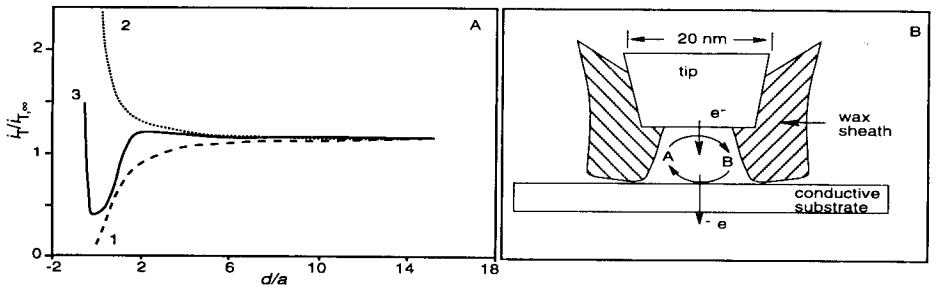

FIG. 5 - (A) SECM approach curves. (1) Disk-shaped tip, insulating substrate. (2) Disk-shaped tip, conductive substrate. (3) Recessed tip, conductive substrate. (B) Schematic of single-molecule detection with the SECM. Molecule A is trapped between tip and substrate. (From reference 25.)

It is not currently possible to measure the charge or current from single electron-transfer events at an electrode. To detect a single molecule electrochemically, one must provide an amplification process. In the SECM experiment, illustrated in Figure 5B, this amplification is provided by the positive feedback process, i.e., the repeated conversion of A to B at the tip and B to A at the substrate as the molecule, in the oxidized or reduced state, shuttles back and forth between tip and substrate. The transport between the two electrodes is by diffusion, so that the transit time, τ, between tip and surface separated by a distance d is about $d^2/2D$ (D is the diffusion coefficient of the redox species). If d = 10 nm and $D = 10^{-5}$ cm^2/s, then $\tau = 5 \times 10^{-8}$ s or the molecule cycles 10^7 times per second. If each cycle results in the exchange of one electron (1.6×10^{-19} C), then an average current of about 1.6 pA will flow. Thus positive feedback provides a ten-million fold amplification that results in a readily measurable current. It is necessary, however, to trap the molecule within the small pocket formed by the surrounding insulator in the gap between tip and substrate for a sufficient time to make the measurement, and this is governed by the time constant of the picoammeter.

Figure 6A shows an experiment with a water-soluble ferrocene derivative as the species oxidized at the tip to produce the ferrocenium form that is then reduced at the indium tin oxide (ITO) substrate.[23] In this experiment, the tip with a radius of about 10 nm was brought to a position where the tip current (see curve 3 of Figure 5A) was near its minimum value, estimated d at about 10 nm.

At the concentration of electroactive species employed, the resultant volume under the tip would contain, on the average, one molecule of ferrocene. Fluctuations of the current at the tip (recorded vs time) were interpreted to indicate the presence of 0, 1, or 2 molecules. Autocorrelation and probability density function analyses (Figure 6B and 6C) of the data were used to confirm this.[24] Control experiments with the tip at longer and closer distances to the ITO and with two different species that oxidize at two different potentials (e.g., ferrocene and $Os(bpy)_3^{2+}$) are consistent with this interpretation. The increase in current shown in curve 1 of Figure 6A signals the entrance of an electroactive molecule into the tip/ITO gap. The fact that the signal rises more slowly than one would expect is attributed to a slow continuous drift of the tip toward and away from the substrate, probably caused by thermal fluctuations and mechanical relaxation of the piezo-elements, which would superimpose a long term rise and fall in the tip current. One can also use an *n*-type semiconductor, e.g., TiO_2, as a substrate.[24] By controlling the potential of the semiconductor, it can be made to behave as either a conductor (in the accumulation region) or an insulator (in the depletion region). Thus, one can show with the same solution and tip that positive feedback and the fluctuating current response occur when the TiO_2 is conductive, but no response is observed when it is insulating.

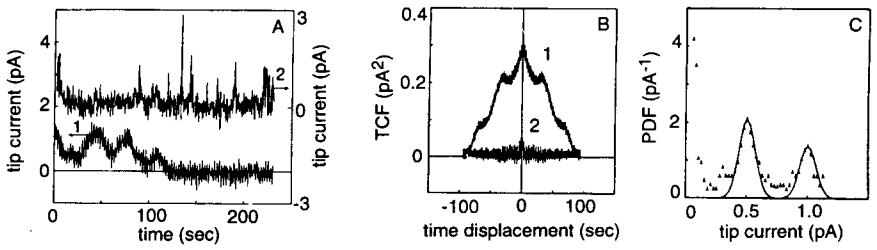

FIG. 6 - (A) Time history record of the tip current observed at a tip potential of 0.55 V and an ITO substrate potential of -0.3 V vs SCE. Tip radius ≈ 7 nm. Curve 1: $d \approx 10$ nm; solution, 2 mM $Cp_2Fe\ TMA^+$ and 2.0 M $NaNO_3$. Curve 2: d is within tunneling range in a solution containing only 2.0 M $NaNO_3$. The data sampling rate was 0.4 s per point. (B) Time correlation function, and (C) probability density function of the time series in A, curve 1. (From reference 24.)

Electron transfer at the interface of two immiscible electrolyte solutions (ITIES)

SECM has been used to study electron transfer (ET) rates at the ITIES.[27-29] ET between two redox species dissolved in different phases (organic and aqueous) was demonstrated by Guainazzi et al. in 1975.[30] However, extraction of the kinetic parameters from conventional electrochemical measurements at the ITIES is complicated by the difficulties of discrimination between ET and ion transfer (IT), distortions from the double-layer charging current and *iR*-drop in highly resistive non-aqueous solvents, and the limited potential window. The use of SECM can eliminate many of these experimental problems.

In a typical SECM-ITIES experime
containing the reduced form of the redox
reacts at the tip surface to produce the ox
the ITIES, the mediator can be regenerate
O_1 in the top phase and R_2 in the bottor

and i_T increases with a decrease in the ti
such a reaction can be evaluated from the
blocks mediator diffusion to the tip, so i_T
studies of the ITIES have been carried ou
measurements, a nonpolarized ITIES is
ions (ClO_4^-) providing a constant drivin
quantitatively separated from IT process
concentration effects and the true potent

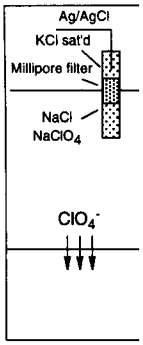

FIG. 7 - Schematic diagram of SE

The rate of ET between the oxidiz
soluble redox mediators ($Ru(CN)_6^{4-}$, M
interface. Both phases contained ClO_4^-
during ET. The ratio of the concentratio
difference ($\Delta_w^o \varphi$) at the liquid junction:

In a typical SECM-ITIES experiment (Figure 7), a tip UME is placed in a top liquid phase containing the reduced form of the redox species, R_1. When the tip is held at a positive potential, R_1 reacts at the tip surface to produce the oxidized form of the species, O_1. When the tip approaches the ITIES, the mediator can be regenerated at the interface via the bimolecular redox reaction between O_1 in the top phase and R_2 in the bottom (aqueous) phase:

$$R_1 - e \rightarrow O_1 \qquad \text{(tip)} \qquad (2)$$

$$O_1 + R_2 \rightarrow R_1 + O_2 \qquad \text{(ITIES)} \qquad (3)$$

and i_T increases with a decrease in the tip-ITIES separation, d (positive feedback). The kinetics of such a reaction can be evaluated from the i_T-d curve.[27,28] If no regeneration of R_1 occurs, the ITIES blocks mediator diffusion to the tip, so i_T decreases at smaller d (negative feedback). Conventional studies of the ITIES have been carried out at externally biased polarized ITIES; in SECM measurements, a nonpolarized ITIES is poised by the concentrations of the potential-determining ions (ClO_4^-) providing a constant driving force for the ET process. In this way, ET can be quantitatively separated from IT processes, allowing unambiguous distinction between the concentration effects and the true potential dependence of the rate constant.

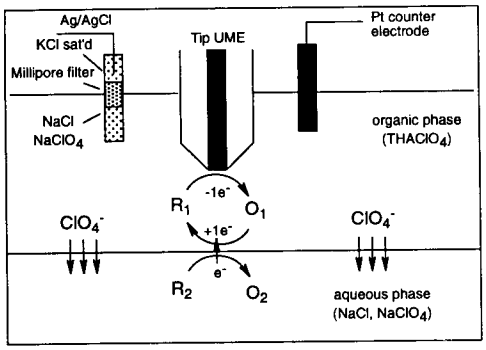

FIG. 7 - Schematic diagram of SECM-ITIES.

The rate of ET between the oxidized form of zinc porphyrin in benzene and different water soluble redox mediators ($Ru(CN)_6^{4-}$, $Mo(CN)_8^{4-}$ and $Fe(CN)_6^{4-}$) was measured at the benzene/water interface. Both phases contained ClO_4^- ions to maintain electroneutrality between the two phases during ET. The ratio of the concentration of ClO_4^- in the two phases determined the galvani potential difference ($\Delta_w^o \varphi$) at the liquid junction:[31]

$$\Delta_w^o \varphi = \Delta_w^o \varphi^\circ_{ClO_4^-} + 0.059\log\frac{[ClO_4^-]_w}{[ClO_4^-]_o} \quad (4)$$

Measurement of rate constant of reaction (3) at constant ClO_4^- concentration in benzene (0.25 M) and at different ClO_4^- concentrations in water (0.01-2 M) yielded the potential dependence for ET at the ITIES for different water mediators.

The dependence of the apparent rate constant k_f on the concentration of redox species and the driving force can be written as:[32]

$$k_f = \text{const}\,[R_2]\exp(-\Delta G^{\neq}/RT) \quad (5)$$

where $\Delta G^{\neq}$ is the free energy barrier (J/mol). For lower overvoltages, a Butler-Volmer-type approximation can be used:

$$\Delta G^{\neq} = -\alpha F(\Delta E^\circ + \Delta_w^o \varphi) \quad (6)$$

where ΔE° is the difference between the standard potentials of two redox couples, F is the Faraday, α is the transfer coefficient, and $\Delta_w^o \varphi$ is the potential drop across the ITIES. ΔE° values between ZnPor and water mediators were determined as the difference in the half wave potentials obtained from cyclic voltammetry at a 25-μm-diameter Pt microelectrode. The combination of equations (5) and (6) at a fixed concentration of aqueous mediator yields:

$$k_f = \text{const}\exp\{\alpha(\Delta E^\circ + 0.06\log[ClO_4^-]_w)/f\} \quad (7a)$$

or

$$\ln(k_f) = \text{const} + \alpha(\Delta E^\circ + 0.06\log[ClO_4^-]_w)/f \quad (7b)$$

where $f = RT/F$. Thus, the $\log(k_f)$ vs $(\Delta E^\circ + 0.06\log[ClO_4^-]_w)$ dependence for different redox couples should be linear with a slope proportional to α. In agreement with equation (7b), linear plots of $\log(k_f)$ vs $(\Delta E^\circ + 0.06\log[ClO_4^-]_w)$ were obtained for $Ru(CN)_6^{4-}$ at higher concentrations of ClO_4^-, corresponding to less negative $\Delta_w^o \varphi$ (Figure 8). At lower $[ClO_4^-]_w$, corresponding to a more positive $\Delta_w^o \varphi$, the ET rate approached the limit corresponding to the rate of $ZnPor^+$ diffusion in the UME/interface gap, and the curves tended to level off. This effect is more significant at higher concentrations of $Ru(CN)_6^{4-}$, for which the k_f values (at the same $\Delta_w^o \varphi$) are higher. Two similar transfer coefficient values were found from the linear portions of these plots, i.e., $\alpha = 0.49 \pm 0.1$ for 50 mM $Ru(CN)_6^{4-}$ and $\alpha = 0.56 \pm 0.05$ for 7 mM $Ru(CN)_6^{4-}$. Data obtained for $Mo(CN)_8^{4-}$ are

quite close to that for $Ru(CN)_6^{4-}$ and sho
level off at higher$[ClO_4^-]$. For ET betwe
value obtained for the rate constant corre

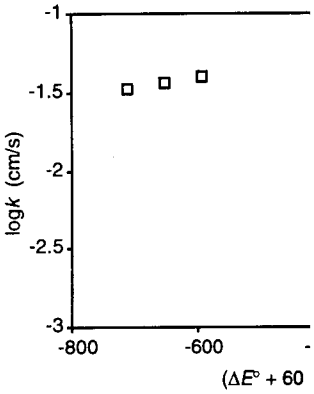

FIG. 8 - Effective heterogeneous r
and the difference in stanc
The top phase was a 0.25
bottom phase was an aque
mediator as indicated in th

Our studies also suggest that the re
boundary. Clearly, the potential depend
between two reacting molecules and the
the ET reaction occurred within a fairly t
interfacial boundary, this potential drop
$\Delta_w^o\varphi$ value. This would have resulted in

SECM can also be used to study ad
at the liquid/liquid interface forming a we
concentration of lipid in benzene (when c
ET for low ΔE° (between $ZnPor^+$ and Ru
$Fe(CN)_6^{4-}$). When a complete monolaye
smaller than can be measured by SECM
rate constant across the monolayer reach
rate of ET across a monolayer strongly d
9B). This allows us to assume that ET in
monolayer rather than by ET at defects a

quite close to that for $Ru(CN)_6^{4-}$ and show a potential dependence at low $[ClO_4^-]$ in water and then level off at higher$[ClO_4^-]$. For ET between $ZnPor^+$ and $Fe(CN)_6^{4-}$, ΔE° is very negative and the value obtained for the rate constant corresponds to the diffusion limit.

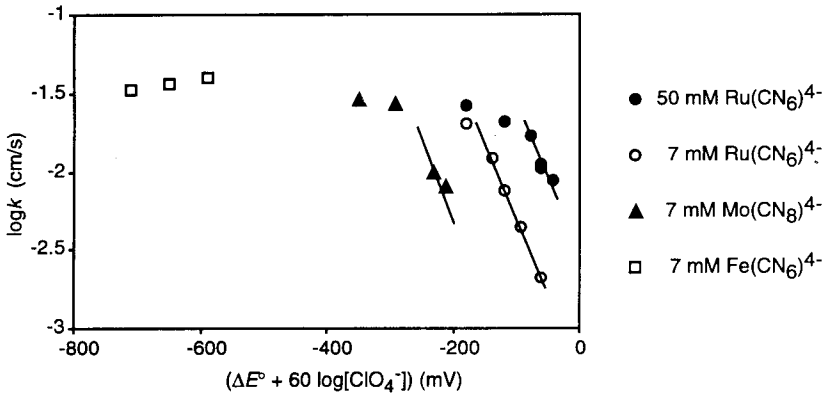

FIG. 8 - Effective heterogeneous rate constant as a function of potential drop across the ITIES and the difference in standard potential between $ZnPor^+$ and different redox mediators. The top phase was a 0.25 M $THAClO_4$ and 0.5 mM ZnPor benzene solution. The bottom phase was an aqueous solution of 0.1 M NaCl, 0.01-2 M $NaClO_4$, and redox mediator as indicated in the figure legend.

Our studies also suggest that the reactants do not significantly penetrate the interfacial boundary. Clearly, the potential dependence of the ET rate is related to the potential drop that exists between two reacting molecules and the difference in the standard potentials of the redox species. If the ET reaction occurred within a fairly thick mixed solvent layer rather than across the thin interfacial boundary, this potential drop would be negligible or at least much smaller than the total $\Delta_w^o\varphi$ value. This would have resulted in $\alpha << 0.5$.

SECM can also be used to study adsorption at the ITIES. Lipid molecules are readily adsorbed at the liquid/liquid interface forming a well-organized monolayer. Figure 9A shows that, at a low concentration of lipid in benzene (when coverage is far from monolayer), lipid dramatically decreases ET for low ΔE° (between $ZnPor^+$ and $Ru(CN)_6^{4-}$) and for high ΔE° (between $ZnPor^+$ and $Fe(CN)_6^{4-}$). When a complete monolayer is formed, the ET rate constant for low ΔE° becomes smaller than can be measured by SECM (lower than 5×10^{-4} cm/s). However, at higher ΔE°, the ET rate constant across the monolayer reaches the lower limit available for SECM measurements. The rate of ET across a monolayer strongly depends on the length of the lipid hydrocarbon chain (Figure 9B). This allows us to assume that ET in this case occurs mainly by tunneling across the lipid monolayer rather than by ET at defects and holes in the film.

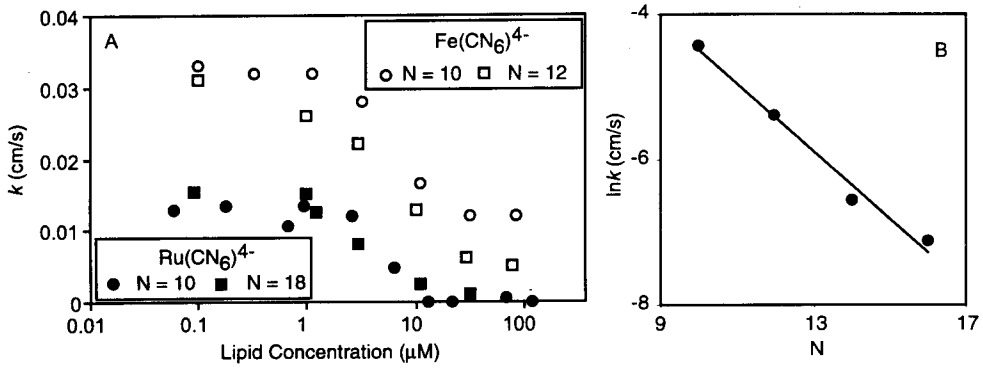

FIG. 9 - (A) Dependence of effective heterogeneous rate constant on lipid concentration in benzene. The top phase was a 0.25 M $THACIO_4$ and 0.5 mM ZnPor in a benzene solution containing lipid. The bottom phase was an aqueous solution of 0.1 M NaCl, 0.01-2 M $NaClO_4$, and 7 mM redox mediator. N = number of carbon atoms in paraffinic chain of lipids. (B) Dependence of effective heterogeneous rate constant of ET between $ZnPor^+$ and $Fe(CN)_6^{4-}$ across a lipid monolayer on the number of carbon atoms in the lipid hydrocarbon chains.

SECM studies of ECE/DISP reactions

SECM can be used as an efficient tool for studying the kinetics and mechanism of reactions following electron transfer.[13, 33-36] First-order[13] (EC) and second-order[33,35,36] (EC_{2i}) reactions have been studied using this technique, and we have now begun to study the use of SECM for reactions in which two electrons are transferred. These reactions can be represented globally by the following scheme (written here for a cathodic process):

$$\text{Electrode :} \quad A + e^- \rightarrow B \tag{8}$$

$$\text{Solution:} \quad B \xrightarrow{k} C \tag{9}$$

$$\text{Electrode:} \quad C + e^- \rightarrow D \tag{10}$$

The second electron transfer can occur at the electrode as represented by reaction 10 (ECE scheme), but can also occur in solution in the following disproportionation reaction (DISP1 scheme):[37-40]

$$\text{Solution : } C + B \xrightarrow{\text{fast}} A + D \tag{11}$$

This results in the regeneration of A which is then reduced at the electrode, leading also to an overall two-electron process. The SECM can discriminate between the ECE and DISP1 pathways, and the appropriate kinetic constants can be obtained from the SECM response.[41]

In this application of the SECM, the electroactive to a potential where the redu than A, so its reduction at the tip (conside controlled. The substrate is held at a potei the assumption that C is much easier to r which is also at the substrate electrode, o potential is not very positive of the A/B v within the tip-substrate domain in the cas schematically in Figure 10.

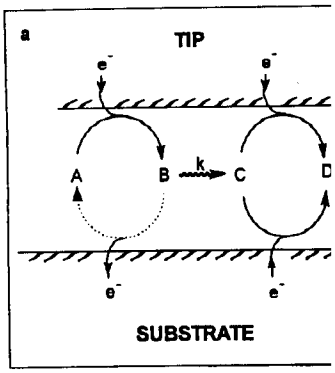

FIG. 10 - Diffusional and chemical case of (a) an ECE pathw

A competition is established betwe feedback of A to the tip) and the first-or brought close to the substrate, the prese A to the tip which diminishes the tip cu diffusion time of B across the gap is sm which results in an increase of the tip cu regimes allows the determination of the

Figure 10 also shows that the mea mode can provide a potential route for t conversion of C to D at the substrate in

Figure 11 shows the theoretical ap using the ADI simulation technique;[42] t kinetic constant $K = ka^2/D = 10$ (a is th ECE-case, the substrate current change ability of C to be reduced at the substra

In this application of the SECM, the tip UME is scanned from a potential where A is not electroactive to a potential where the reduction of A is diffusion-controlled. C is more easily reduced than A, so its reduction at the tip (considered only in the case of the ECE pathway) is also diffusion-controlled. The substrate is held at a potential where the oxidation of B is diffusion-controlled. With the assumption that C is much easier to reduce than A, we must consider that the reduction of C, which is also at the substrate electrode, occurs at a diffusion-controlled rate, when the substrate potential is not very positive of the A/B wave. The diffusional and chemical processes occurring within the tip-substrate domain in the case of an ECE and a DISP1 pathways are shown schematically in Figure 10.

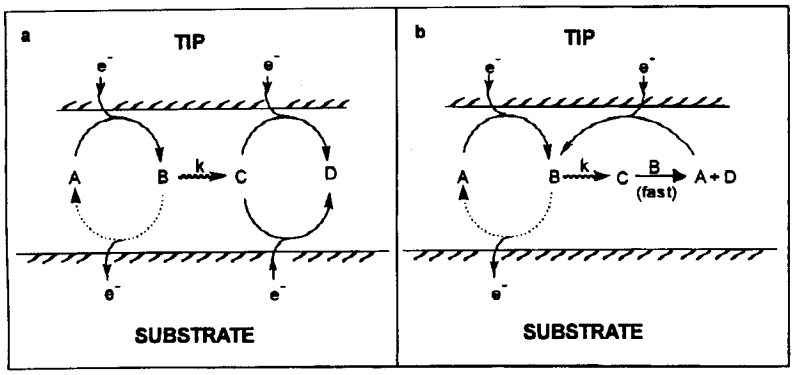

FIG. 10 - Diffusional and chemical processes occurring within the tip-substrate domain in the case of (a) an ECE pathway and (b) a DISP1 pathway. (Reprinted from reference 41.)

A competition is established between the diffusion of B to the substrate (leading to the feedback of A to the tip) and the first-order chemical reaction (equation 9). When the electrode is brought close to the substrate, the presence of the substrate first results in the hindered diffusion of A to the tip which diminishes the tip current. At very close tip-substrate separation, when the diffusion time of B across the gap is small compared to its lifetime, the substrate regenerates A, which results in an increase of the tip current. The observation of the transition between those two regimes allows the determination of the kinetic rate of the homogeneous reaction.

Figure 10 also shows that the measurement of the substrate current in the generation/collection mode can provide a potential route for the discrimination between the two mechanisms, since the conversion of C to D at the substrate in the ECE mechanism causes a cathodic current to flow.

Figure 11 shows the theoretical approach curves obtained for the ECE and DISP1 reactions using the ADI simulation technique;[42] these curves were calculated with a value of the dimensionless kinetic constant $K = ka^2/D = 10$ (a is the electrode radius and D the diffusion coefficient). In the ECE-case, the substrate current changes sign as the tip-substrate separation decreases due to the ability of C to be reduced at the substrate. This change of sign of the substrate current is not

observed in the DISP1 case and can therefore be used as an experimental diagnostic to establish the occurrence of an ECE pathway.

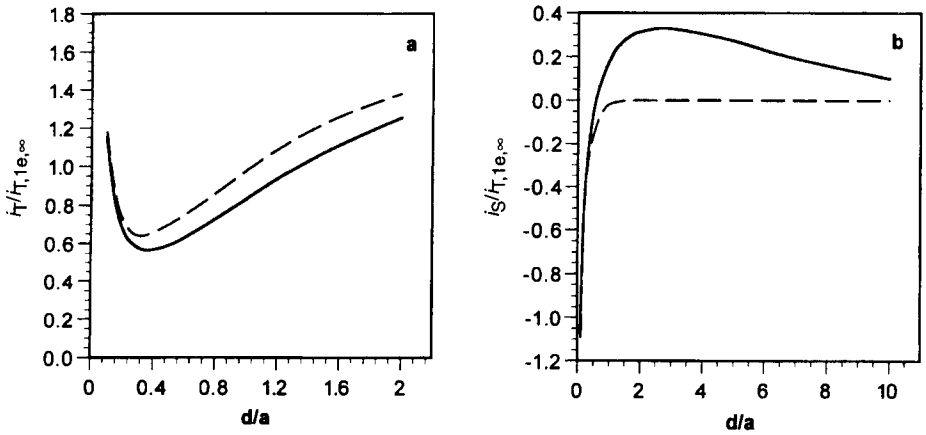

FIG. 11 - Comparison between the approach curves obtained for the ECE case (—) and the DISP1 case (---) for $K = 10$. (a) Tip and (b) substrate current as a function of the dimensionless tip-substrate separation. (Data from reference 41.)

In the presence of phenol, anthracene undergoes a two-electron reduction leading to 9,10-dihydroanthracene. This two-electron reduction follows a DISP1 pathway[39] and can be represented by the following reaction sequence:

$$A + e^- \rightleftarrows A^{\cdot -} \quad (12)$$

$$A^{\cdot -} + PhOH \xrightarrow{k'} AH^{\cdot} + PhO^- \quad (13)$$

$$AH^{\cdot} + A^{\cdot -} \xrightarrow{k_d} AH^- + A \quad (14)$$

$$AH^- + PhOH \xrightarrow{fast} AH_2 + PhO^- \quad (15)$$

$$A + 2e^- + 2PhOH \rightleftarrows AH_2 + 2PhO^- \quad \text{(overall)} \quad (16)$$

where A represents anthracene and PhOH, phenol.

In the presence of an excess of phenol, reaction 13 can be considered as a pseudo-first-order reaction. SECM experiments can therefore lead to the determination of the rate constant k' corresponding to the protonation of the anthracene radical anion by phenol. Figure 12 shows the experimental approach curves obtained for different phenol concentrations.

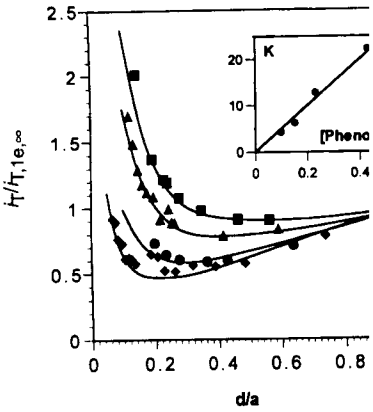

FIG. 12 - Reduction of anthracene in substrate dimensionless cur inset represents the experim concentration. (Data from re

The main feature of the experimental decreasing tip-substrate distance. This poi work.[39] From the best fit between the exp the value of $K = k'[PhOH]a^2/D$ at each phe values versus the corresponding phenol co constant for the protonation of the anthrac M^{-1} s^{-1}. This value is in very good agreem $(\pm 0.8) \times 10^3$ M^{-1} s^{-1}.[39] Thus, SECM can rate-determining step in chemical reaction DISP1 pathways.

SECM continues to find new applic electroanalytical chemistry. It is also bein skin), polymers, membranes, and solid cr this paper, potentiometric (ion selective e species that do not produce a voltammetr pursuing SECM studies;[43] the work discu laboratory. Although there is currently n available in 1997.

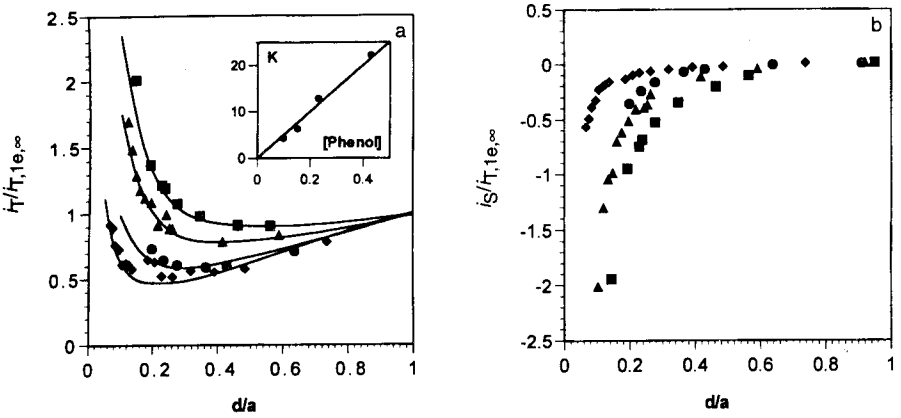

FIG. 12 - Reduction of anthracene in the presence of phenol in DMF. Typical (a) tip and (b) substrate dimensionless currents measured at different tip-substrate separation. The inset represents the experimental value of K as a function of the corresponding phenol concentration. (Data from reference 41.)

The main feature of the experimental data is that the substrate current doesn't change sign with decreasing tip-substrate distance. This points to a DISP1 pathway, in agreement with previous work.[39] From the best fit between the experimental tip current and the theoretical approach curves, the value of $K = k'[\mathrm{PhOH}]a^2/D$ at each phenol concentration can be determined. By plotting these values versus the corresponding phenol concentration (see inset of Figure 12), we determined the rate constant for the protonation of the anthracene radical anion by phenol to be $k' = 4.4\ (\pm\ 0.4) \times 10^3$ $M^{-1}\ s^{-1}$. This value is in very good agreement with the value previously reported in the literature 4.8 $(\pm\ 0.8) \times 10^3\ M^{-1}\ s^{-1}$.[39] Thus, SECM can be used to accurately determine the kinetic constant of the rate-determining step in chemical reactions and can also be used to distinguish between ECE and DISP1 pathways.

CONCLUSIONS

SECM continues to find new applications in many areas of electrochemistry and electroanalytical chemistry. It is also being used to study biological surfaces (e.g., leaf surfaces and skin), polymers, membranes, and solid crystals. In addition to the amperometric tips discussed in this paper, potentiometric (ion selective electrode) and enzyme tips have been applied to monitor species that do not produce a voltammetric response (e.g., H^+, K^+). A number of research groups are pursuing SECM studies;[43] the work discussed in this paper focuses on recent results from our laboratory. Although there is currently no commercial SECM, one is being developed and should be available in 1997.

Acknowledgments - The contributions of J. Kwak, M. V. Mirkin, and P. R. Unwin to the research described in this paper and the assistance of Rose McCord in the preparation of this manuscript are gratefully acknowledged. Our research on SECM has been sponsored by the Robert A. Welch Foundation and the National Science Foundation.

Received September 6th, 1996

REFERENCES

1) A. J. BARD, F.-R. F. FAN, J. KWAK, and O. LEV : *Anal. Chem.*, **61**, 132 (1989).
2) R. M. WIGHTMAN and D. O. WIPF in *Electroanalytical Chemistry*, Vol. 15 (A. J. BARD, Ed.), Marcel Dekker, New York, 1988, p. 267.
3) A. J. BARD, G. DENUAULT, C. LEE, D. MANDLER, and D. O. WIPF : *Acc. Chem. Res.*, **23**, 357 (1990).
4) A. J. BARD, F.-R. F. FAN, D. T. PIERCE, P. R. UNWIN, D. O. WIPF, and F. ZHOU : *Science*, **254**, 68 (1991).
5) M. ARCA, A. J. BARD, B. R. HORROCKS, T. C. RICHARDS, and D. A. TREICHEL : *Analyst*, **119**, 719 (1994).
6) A. J. BARD, F.-R. F. FAN, and M. V. MIRKIN in *Electroanalytical Chemistry*, Vol. 18 (A. J. BARD, Ed.), Marcel Dekker, New York, 1994, p. 244
7) M. V. MIRKIN : *Anal. Chem.*, **68**, 177A (1996).
8) J. KWAK and A. J. BARD : *Anal. Chem.*, **61**, 1221 (1989).
9) M. V. MIRKIN and A. J. BARD : *J. Electroanal. Chem.*, **323**, 1 (1992).
10) M. V. MIRKIN and A. J. BARD : *J. Electroanal. Chem.*, **323**, 29 (1992).
11) A. J. BARD, M. V. MIRKIN, P. R. UNWIN, and D. O. WIPF : *J. Phys. Chem.*, **96**, 1861 (1992).
12) A. J. BARD, G. DENUAULT, R. A. FRIESNER, B. C. DORNBLASER, and L. S. TUCKERMAN : *Anal. Chem.*, **63**, 1282 (1991).
13) P. R. UNWIN and A. J. BARD : *J. Phys. Chem.*, **95**, 7814 (1991).
14) D. O. WIPF and A. J. BARD : *J. Electrochem. Soc.*, **138**, 469 (1991).
15) D. O. WIPF and A. J. BARD : *Anal. Chem.*, **64**, 1362 (1992).
16) D. O. WIPF and A. J. BARD : *Anal. Chem.*, **65**, 1373 (1993).
17) A. C. HILLIER and M. D. WARD : *Anal. Chem.* **64**, 2539 (1992).
18) D. MANDLER and A. J. BARD : *J. Electrochem. Soc.* **136**, 31 (1989).
19) C. JEHOULET, Y. S. OBENG, Y.-T. KIM, F. ZHOU, and A. J. BARD : *J. Am. Chem. Soc.*, **114**, 4237 (1992).
20) (a) F. ZHOU, S.L. YAU, C. JEHOULET, D.A. LAUDE, Z. GUAN, and A.J. BARD : *J. Phys. Chem.*, **96**, 4160 (1992). (b) W. KOH, D. DUBOIS, W. KUTNER, M. T. JONES, and K. M. KADISH : *J. Phys. Chem.*, **97**, 6871 (1993).
21) J. CHLISTUNOFF, D. CLIFFEL, and A. J. BARD : *Thin Solid Films*, **257**, 166 (1995).
22) (a) J. L. ATWOOD, G. A. KOL
(b) T. SUZUKI, K. NAKASHI
23) F.-R. F. FAN and A. J. BARD :
24) F.-R. F. FAN, J. KWAK, and A
25) A. J. BARD and F.-R. F. FAN
26) L. A. NAGAHARA, T. THUN
(1989).
27) C. WEI, A. J. BARD, and M.
28) M. TSIONSKY, A. J. BARD,
29) Y. SELZER and D. MANDLEI
30) M. GUAINAZZI, G. SILVEST
200 (1975).
31) H. H. GIRAULT and D. J. SCH
Ed.), Marcel Dekker, New Yor
32) R. A. MARCUS : *J. Phys. Che*
33) F. ZHOU, P. R. UNWIN, and
34) P. R. UNWIN and A. J. BARD
35) D. A. TREICHEL, M. V. MIR
36) F. ZHOU and A. J. BARD : *J.*
37) M. D. DALE and S. W. FELDI
38) C. P. ANDRIEUX and J.-M. S
39) (a) C. AMATORE, M. GAREI
and references therein. (b) C. A
353 (1980).
40) M. FLEISCHMANN, F. LASS
(1984).
41) C. DEMAILLE, P. R. UNWIN
42) D. W. PEACEMAN and H. H.
43) See references 3-7 for reviews

22) (a) J. L. ATWOOD, G. A. KOUTSANTONIS, and C. L. RASTON : *Nature,* **368**, 229 (1994). (b) T. SUZUKI, K. NAKASHIMA, and S. SHINKAI : *Chem. Lett.*, 699 (1994).
23) F.-R. F. FAN and A. J. BARD : *Science,* **267**, 871 (1995).
24) F.-R. F. FAN, J. KWAK, and A. J. BARD : *J. Am. Chem. Soc.* (in press).
25) A. J. BARD and F.-R. F. FAN : *Acc. Chem. Res.* (submitted).
26) L. A. NAGAHARA, T. THUNDAT, and S. M. LINDSAY : *Rev. Sci. Instrum.,* **60**, 3128, (1989).
27) C. WEI, A. J. BARD, and M. V. MIRKIN : *J. Phys. Chem.,* **99**, 16033 (1995).
28) M. TSIONSKY, A. J. BARD, and M. V. MIRKIN : *J. Phys. Chem.* (submitted).
29) Y. SELZER and D. MANDLER : *J. Electroanal. Chem.*, **409**, 15 (1996).
30) M. GUAINAZZI, G. SILVESTRY, and G. J. SURVALLE : *Chem. Soc. Chem. Commun.* **1975**, 200 (1975).
31) H. H. GIRAULT and D. J. SCHIFFRIN, in *Electroanalytical Chemistry,* Vol. 15 (A. J. Bard, Ed.), Marcel Dekker, New York, 1989, p. 1.
32) R. A. MARCUS : *J. Phys. Chem.*, **94**, 4152 (1990).
33) F. ZHOU, P. R. UNWIN, and A. J. BARD : *J. Phys. Chem.*, **96**, 4917 (1992).
34) P. R. UNWIN and A. J. BARD : *J. Phys. Chem.*, **96**, 5035 (1992).
35) D. A. TREICHEL, M. V. MIRKIN, and A. J. BARD : *J. Phys. Chem.*, **98**, 5751 (1994).
36) F. ZHOU and A. J. BARD : *J. Am. Chem. Soc.*, 116, **393** (1994).
37) M. D. DALE and S. W. FELDBERG : *J. Phys. Chem.*, **70**, 3459 (1966).
38) C. P. ANDRIEUX and J.-M. SAVÉANT : *J. Electroanal. Chem.*, **267**, 15 (1989).
39) (a) C. AMATORE, M. GAREIL, and J.-M. SAVÉANT : *J. Electroanal. Chem.*, **147**, 1 (1983) and references therein. (b) C. AMATORE and J.-M. SAVÉANT : *J. Electroanal. Chem.*, **107**, 353 (1980).
40) M. FLEISCHMANN, F. LASSERRE, and J. ROBINSON : *J. Electroanal. Chem.*, **177**, 115 (1984).
41) C. DEMAILLE, P. R. UNWIN, and A. J. BARD : *J. Phys. Chem.*, (in press).
42) D. W. PEACEMAN and H. H. RACHFORD : *J. Soc. Ind. Appl. Math.*, **3**, 28 (1995).
43) See references 3-7 for reviews of SECM.